CrossMark
click for updates

Real-time monitoring of plasmon induced dissociative electron transfer to the potential DNA radiosensitizer 8-bromoadenine†

R. Schürmann[a,b] and I. Bald*[a,b]

The excitation of localized surface plasmons in noble metal nanoparticles (NPs) results in different nano-scale effects such as electric field enhancement, the generation of hot electrons and a temperature increase close to the NP surface. These effects are typically exploited in diverse fields such as surface-enhanced Raman scattering (SERS), NP catalysis and photothermal therapy (PTT). Halogenated nucleobases are applied as radiosensitizers in conventional radiation cancer therapy due to their high reactivity towards secondary electrons. Here, we use SERS to study the transformation of 8-bromoadenine ([8Br]A) into adenine on the surface of Au and AgNPs upon irradiation with a low-power continuous wave laser at 532, 633 and 785 nm, respectively. The dissociation of [8Br]A is ascribed to a hot-electron transfer reaction and the underlying kinetics are carefully explored. The reaction proceeds within seconds or even milli-seconds. Similar dissociation reactions might also occur with other electrophilic molecules, which must be considered in the interpretation of respective SERS spectra. Furthermore, we suggest that hot-electron transfer induced dissociation of radiosensitizers such as [8Br]A can be applied in the future in PTT to enhance the damage of tumor tissue upon irradiation.

Introduction

Illumination of noble metal nanoparticles (NPs) with visible light leads to resonant oscillations of the electron gas, which are referred to as localized surface plasmons (LSP). In close proximity to the metal surface the electric field of the incoming and scattered light is highly enhanced by the LSP, which is exploited in surface enhanced Raman scattering (SERS), as the Raman scattering cross sections increase by several orders of magnitude.[1,2] LSP can relax inelastically *via* reemitting a photon or through a non-radiative channel *via* electron hole pair production.[3,4] These so called "hot electrons" can tunnel into unoccupied molecular orbitals of chemisorbed or physisorbed molecules and induce chemical reactions[5–9] that can be monitored in real time using SERS.[10,11]

Besides the direct electron transfer that is exploited in plasmonic catalysis "hot electrons" lose their energy very quickly *via* electron–electron scattering and subsequently *via* electron phonon scattering, which increases the temperature of the nanoparticles and their surroundings.[12] In photothermal therapy (PTT) the increased temperature around hollow AuNPs[13] or nanorods[14] is used to kill cancer cells under illumination with NIR-lasers.[15,16] Based on the work presented here we suggest that the combination of NPs with molecules incorporated in the DNA that strongly react with plasmon induced electrons might improve the efficiency of this therapy. Such potential radiosensitizers are halogenated nucleobases like 8-bromoadenie ([8Br]A) that strongly interact with low energy electrons[17–20] *via* dissociative electron attachment (DEA)[21] whereby a transient negative ion decays into anionic and neutral fragments. This mechanism allows the damage of DNA below the ionization threshold.[22] Brominated nucleobases that can be easily incorporated into the DNA possess a high electron affinity and the C–Br-bond is easily cleaved by attachment of electrons close to 0 eV.[23,24] The formation of a radical inside the DNA leads to a strand break in a second step[25] and thus increases the single strand break cross section.[26]

Here we demonstrate the dissociative hot electron transfer from plasmonically excited Au and AgNPs to [8Br]A in a dry and aqueous environment monitored in real time using SERS. The reaction follows a fractal like kinetics and shows a fast reaction rate, as under typical SERS settings the majority of the analyte molecules are decomposed in a few hundred milliseconds.

[a]*Institute of Chemistry, Physical Chemistry, University of Potsdam, Karl-Liebknecht-Str. 24-25, 14776 Potsdam, Germany. E-mail: bald@uni-potsdam.de*
[b]*BAM Federal Institute for Materials Research and Testing, Richard-Willstätter-Str. 11, 12489 Berlin, Germany*
†Electronic supplementary information (ESI) available. See DOI: 10.1039/c6nr08695k
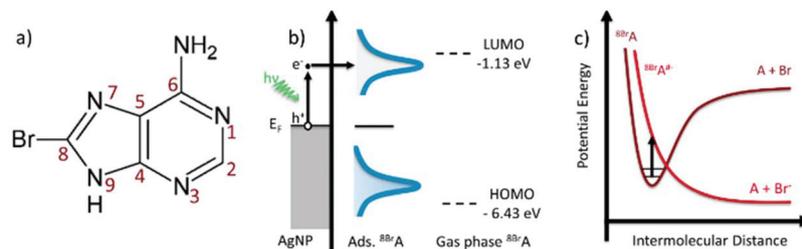
Fig. 1 (a) Molecular structure of ^{8Br}A; (b) schematic "hot electron" excitation in the silver nanoparticle with subsequent tunnelling into the LUMO of the adsorbed ^{8Br}A; (c) schematic potential energy diagram illustrating DEA to ^{8Br}A.

Results and discussion

LSP that are created *via* laser illumination of AgNPs can decay non-radiatively by the formation of an electron hole pair, whereby the electron is excited from the sp-conduction band and has an energy between E_f and $E_f + h\nu$ (Fig. 1):

$$h\nu + AgNP \rightarrow e^- + h^+ \tag{1}$$
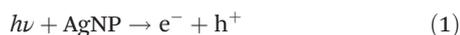
On a time scale below 10 fs the excited electron loses its energy *via* electron–electron scattering until the electron gas approaches a Fermi–Dirac distribution.[3] These so called "hot electrons" can tunnel into the lowest unoccupied molecular orbital (LUMO) of adsorbed ^{8Br}A molecules and form a transient negative ion (TNI).[21] Beyond that the electron can be directly injected into the LUMO *via* a coherent tunneling process before the electron interacts with the electron gas.[27,28] In both cases a relatively unstable ^{8Br}A anion is formed that can relax through the cleavage of the C8–Br bond.[17,18]

$$^{8Br}A + e^- \rightarrow {}^{8Br}A^{\#-} \rightarrow A^{\bullet} + Br^- \tag{2}$$
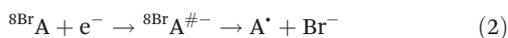
In the present experiment a AgNP solution with adsorbed ^{8Br}A was dried on a Si wafer and SERS spectra were recorded as a function of the illumination time using a 532 nm laser with 250 µW focused on a 10 µm diameter spot. For a relatively short time of around 1 s Raman spectra were recorded with a band structure that is clearly assigned to ^{8Br}A (Fig. 2a). The most remarkable bands are the ring breathing mode at 767 cm^{-1} and the C–Br bending- and stretching-mode at 299 cm^{-1} and 575 cm^{-1}, respectively. With ongoing illumination, these bands are significantly decreasing in their intensity while simultaneously new bands arise at 336 cm^{-1}, 629 cm^{-1},

735 cm^{-1}, 967 cm^{-1}, 1267 cm^{-1}, 1329 cm^{-1}, 1409 cm^{-1}, 1465 cm^{-1} and 1575 cm^{-1} (indicated by a grey background in Fig. 2) that can be assigned to the SERS-spectrum of adenine (A).[29] This indicates that the C–Br bond of the adsorbed ^{8Br}A ruptures during laser irradiation most likely due to the dissociative attachment of an additional electron according to eqn (2). By capture of an H radical from the environment A is formed on the nanoparticle surface. A similar reaction has previously been demonstrated already with uracil.[24] The transformation from ^{8Br}A to A can be tracked by the intensity of the ring breathing mode at 735 cm^{-1} and 767 cm^{-1} (Fig. 2c).

The rate of the reaction depends on the concentration of ^{8Br}A and the concentration of "hot electrons" in the illuminated area:

$$\text{Rate} = -k \left[{}^{8Br}A\right] \left[e^-\right] \tag{3}$$

However, it is difficult to monitor both concentrations simultaneously, in particular the number of hot electrons remains unknown. During continuous laser irradiation, a constant equilibrium concentration of "hot electrons" can be assumed as they are frequently reproduced and their time-scales for excitation and relaxation are several orders of magnitude shorter than the timescales of the DEA reaction. Hence pseudo first-order kinetics is assumed to determine the observed rate coefficient k_{obs} of the dissociation of ^{8Br}A:

$$k_{obs} = \frac{1}{t} \cdot \ln \frac{\left[{}^{8Br}A\right]_0}{\left[{}^{8Br}A\right]_t} \tag{4}$$

In Fig. 3a k_{obs} is plotted against time t, which demonstrates that the rate coefficient is not constant as expected for a (pseudo-) first order reaction, but decreases in time. This is
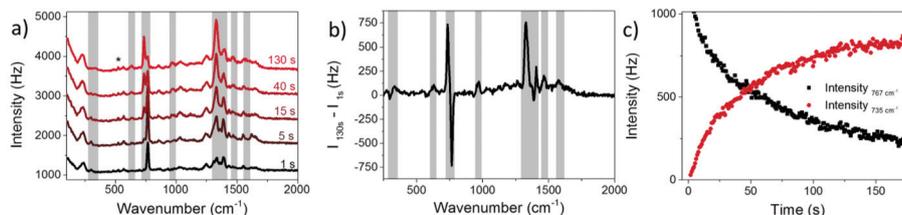
Fig. 2 (a) SERS spectra of ^{8Br}A on AgNPs dried on a Si-substrate for different illumination times. The Si band from the substrate at 521 cm^{-1} is marked with a *. (b) Difference spectra of $t = 1$ s and $t = 130$ s (same data set like in a). (c) Intensity of ring-breathing mode of ^{8Br}A at 767 cm^{-1} *vs.* ring breathing mode of A at 735 cm^{-1}.
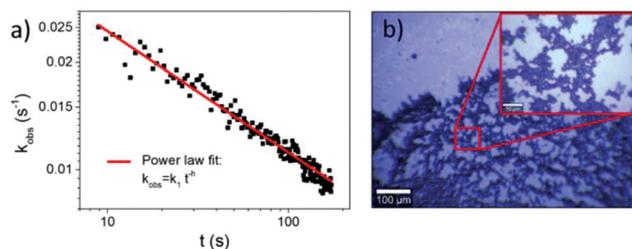
Fig. 3 (a) Observed rate coefficient plotted against illumination time shows a power law dependence with $h = 0.34 \pm 0.01$. (b) Light microscopy image of a dried AgNP sample on Si reveals a fractal structure of aggregated AgNPs.

attributed to the inhomogeneous distribution of reaction sites on the surface giving rise to a broad range of signal intensities and thus rate constants. In close proximity to the noble metal surface the electric field of the incoming and scattered light is strongly increased due to its interaction with the LSP, which strongly depends on the arrangement and structure of the nanoparticles. This electromagnetic enhancement increases the intensity of the Raman signal (I_j) by some orders of magnitude:[1]

$$I_j = \alpha^2 \cdot g_j^4 \cdot I_0 \tag{5}$$

where α is the Raman scattering cross section, g_j is the electromagnetic enhancement factor of a specific reaction site and I_0 is the incoming laser power. The detected Raman signal is the sum of all signals from all molecules in the focused area:

$$I_{SERS} = \sum_j I_j(x, y) \tag{6}$$

When assuming that the concentration of hot electrons at a certain position is in coherence with the magnitude of LSP, the local reaction rate correlates with the electromagnetic enhancement in the "hotspot". Hence the ^{8Br}A molecules that experience the strongest signal enhancement have the highest decomposition probability. Thus, the reaction centers with the highest rates only contribute in the beginning to the overall reaction, and consequently the observed reaction rate decreases with time.

This time dependence can be characterized by fractal-like kinetics,[30] which describes heterogeneous reactions with geometrical constraints like hot electron catalyzed reactions,[31] with a time dependent rate coefficient:

$$k_{obs} = k_1 \cdot t^{-h}, 0 \leq h \leq 1, t \geq 1, \tag{7}$$

where h is the fractal dimension of the system, t is the time/1 s and k_1 is the rate coefficient at $t = 1$.

According to eqn (4) k_{obs} strongly depends on the starting intensity of the ^{8Br}A signal that rapidly decreases during the first integration time. Assuming that the Raman enhancement factors of ^{8Br}A and A are equivalent the sum of the intensities at 735 cm^{-1} and 767 cm^{-1} was used to determine the starting intensity of the 767 cm^{-1} peak.

20 measurements on the same sample at different positions have been performed and h was determined to be $h = 0.36 \pm 0.09$, which indicates a 2-dimensional fractal lattice, for which $h = 0.33$.[30] Fig. 3a shows one of these measurements. The determined fractal dimension is in accordance with the fractal shape of the nanoparticle aggregates, which were observed in the bright field images (Fig. 3b) and described previously.[32,33] It has to be mentioned that the standard deviation of h is larger than the error of h determined from the power law fit, as the composition of aggregates may vary on different positions of the sample.

Since k_1 and h are not independent fitting parameters, h was set to 0.33 to avoid artifacts in the subsequent analysis. The rate constant k_1 was determined as a function of the incident laser power P and fitted with a power function (see Fig. 4a):

$$k_1 = a \cdot P^b \tag{8}$$

The linear correlation between k_1 and P with $b = 0.92 \pm 0.09$ indicates a one photon process that is characteristic for hot electron induced reactions. For (partly) thermally induced reactions a super-linear power law dependence[5] would be expected due to the exponential dependence of the reaction rate on temperature according to the Arrhenius equation. This conclusion is valid as long as the temperature on the AgNPs rises linearly with the incident laser power.[12] Beyond that a direct photoexcitation is also unlikely for low photon fluences (10^2–10^4 W cm^{-2}), because the HOMO–LUMO gap is about 5.3 eV according to *ab initio* calculations performed at the MP2/aug-cc-pVDZ level of theory.[34] Therefore at least 3 photons with 2.33 eV (532 nm) are required to overcome the HOMO–LUMO gap.

We have also studied the transformation from ^{8Br}A to A on a nanoparticle surface for 633 nm and 785 nm laser wavelength as well as on gold nanoparticles (AuNPs). In all cases a linear dependence on the laser power was observed (Fig. S3 in the ESI† and Fig. 4a). This is remarkable as the work functions of AgNPs (4.3 eV) and AuNPs (5.1 eV) are well above the photon energy of 1.61 eV (785 nm). This supports the model of dissociative electron transfer into the low lying LUMO of ^{8Br}A. Normalizing k_1 by the laser power reveals that the reaction rate increases with photon energy and is lower on AuNPs compared
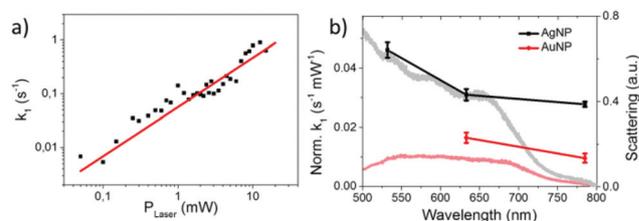
Fig. 4 (a) Rate constant k_1 as a function of the incident laser power fitted by a power law function ($k_1 = a \cdot P_{Laser}^b$ with $b = 0.92 \pm 0.09$). (b) Rate constant normalized by laser intensity for ^{8Br}A dissociation on AgNPs (black) and AuNPs (red) for different laser wavelength and typical dark field spectra of aggregated NPs (grey and light red).
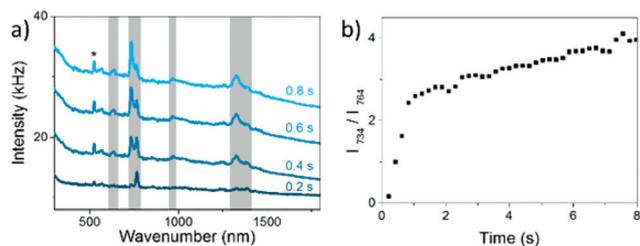
Fig. 5 (a) SERS spectra of ^{8Br}A on AgNPs in aqueous solution taken after different illumination times, irradiated with 785 nm with a power of 5.1 mW. The Si-band is marked with a *. (b) Ratio between ^{8Br}A ring breathing mode at 764 cm^{-1} and A ring breathing mode at 734 cm^{-1} as a function of the illumination time (same data as in a).

to AgNPs (see Fig. 4b) most probably due to the increased plasmonic enhancement on the AgNPs. We have recorded dark field scattering spectra on several spots of the sample, which show a broad surface plasmon resonance (SPR) ranging from around 400 nm for AgNPs and 500 nm for AuNPs to 700 nm. In particular for the near infrared photons with 785 nm wavelength, where the plasmonic enhancement is relatively weak, the SPR does not directly correspond to the normalized k_1, even though the major trends are reflected. This might be explained by a resonant direct electron transfer into the adsorbed ^{8Br}A. Nevertheless, on the basis of the present data it is not possible to say whether the reaction is dominated by a coherent tunnelling process or by Fermi–Dirac distributed electrons scattering into the molecular orbitals of the ^{8Br}A molecule. In order to study the influence of the environment additional measurements have been performed in water using a 785 nm laser with 5.1 mW. Already after less than 400 ms more than half of the ^{8Br}A in the relevant hotspots are dissociated (see Fig. 5). In solution it is difficult to determine accurate rate constants as the photoproduct is diffusing out of the focused area, hence the observed reaction rates represent only an infimum of the real reaction rate. In an aqueous environment the electron tunneling is much more favorable as the tunneling barrier is lowered by 0.8 eV.[35] Therefore, an increased speed of reaction is expected as compared to dry samples.

Conclusions

We demonstrate a dissociative electron transfer from laser illuminated noble metal nanoparticles to the potential DNA radiosensitizer ^{8Br}A dried on a Si substrate as well as in solution. The reaction is described with fractal like kinetics. The observed interaction between the nanoparticles and ^{8Br}A might help to improve photothermal cancer therapy. As the utilized substrate as well as the applied laser settings in this experiment were typical of SERS measurements, the plasmonically catalysed reaction can cause problems in the analysis of the Raman spectra, because the probe laser for the spectral analysis is the same that induces the decomposition of the analyte. As the time scale of the reaction is equivalent or faster than the typical

accumulation time, one has to distinguish carefully between the SERS spectrum of the analyte molecule and its photoproducts. This should be done especially for molecules containing electrophilic groups such as halogens[36,37] or nitro groups,[38] which are known to decompose easily as a consequence of their interaction with "hot electrons".

Experimental section

Chemicals

^{8Br}A was purchased from Carbosynth Ltd (UK) and A, silver nitrate and sodium citrate were purchased from Sigma Aldrich (Germany). All chemicals were diluted in Millipore water and used without further purifications. Gold nanoparticles with a diameter of 40 nm were purchased from BBI solutions.

Silver nanoparticle preparation

AgNPs were prepared by the well-known procedure of Lee and Meisel.[39] Briefly, 50 ml of 1 mM AgNO$_3$ solution were brought to a rolling boil and 5 ml 38.8 mM trisodiumcitrate were added while the boiling was continued for 1 h under rigorous stirring. The produced AgNPs are 36 ± 10 nm in diameter and show an extinction maximum at 413 nm. The size distribution was determined by atomic force microscopy (AFM) using a Nanosurf Flex AFM equipped with a Tap150-Al-G cantilever in the tapping mode and image processing was performed with Gwyddeon 2.39 software. The UV-Vis-spectra were recorded using a Nanodrop 2000 of Thermo scientific.

Surface enhanced Raman spectroscopy

In order to prepare the samples for the Raman measurements 100 µl of a 50 µM ^{8Br}A solution were incubated for 2 h in 400 µl of the AgNP solution. Subsequently the dispersion was centrifuged and the residue was diluted in Millipore water two times. After a final centrifugation step a 2 µl droplet of the nanoparticle solution was dried on an oxygen plasma cleaned Si wafer. For the measurements in a liquid environment a 4 µl droplet was placed on a Si wafer that was surrounded by a bath of Millipore water to reduce the evaporation of the droplet. The Raman spectra were recorded using a Witec alpha 300 Raman-microscope with a 532 nm and a 785 nm laser and a Horiba Labram Raman-microscope with a 633 nm laser. The laser power was varied in the range from 50 µW to 50 mW and focused with a 10× objective on the sample. Scattering spectra of the sample were obtained using the Witec alpha 300 dark field unit with a 50× HD objective from Zeiss. Data analysis and processing were performed with Origin 9.1 software.

Acknowledgements

References

1 M. Moskovits, *J. Raman Spectrosc.*, 2005, **36**, 485–496.

2 J. Prinz, C. Heck, L. Ellerik, V. Merk and I. Bald, *Nanoscale*, 2016, **8**, 5612–5620.

3 G. Baffou and R. Quidant, *Chem. Soc. Rev.*, 2014, **43**, 3898.

4 J. Y. Park, L. R. Baker and G. A. Somorjai, *Chem. Rev.*, 2015, **115**, 2781–2817.

5 P. Christopher, H. Xin, A. Marimuthu and S. Linic, *Nat. Mater.*, 2012, **11**, 1044–1050.

6 S. Mukherjee, F. Libisch, N. Large, O. Neumann, L. V. Brown, J. Cheng, J. B. Lassiter, E. A. Carter, P. Nordlander and N. J. Halas, *Nano Lett.*, 2013, **13**, 240–247.

7 M. J. Kale, T. Avanesian and P. Christopher, *ACS Catal.*, 2014, **4**, 116–128.

8 T. Wadayama and M. Yokawa, *Chem. Phys. Lett.*, 2006, **428**, 348–351.

9 S. M. Kim, S. J. Lee, S. H. Kim, S. Kwon, K. J. Yee, H. Song, G. A. Somorjai and J. Y. Park, *Nano Lett.*, 2013, **13**, 1352–1358.

10 Z. Zhang, T. Deckert-Gaudig and V. Deckert, *Analyst*, 2015, **140**, 4325–4335.

11 W. Xie and S. Schlücker, *Nat. Commun.*, 2015, **6**, 7570.

12 G. Baffou and R. Quidant, *Laser Photonics Rev.*, 2013, **7**, 171–187.

13 A. M. Gobin, M. H. Lee, N. J. Halas, W. D. James, R. A. Drezek and J. L. West, *Nano Lett.*, 2007, **7**, 1929–1934.

14 X. Huang, P. K. Jain, I. H. El-Sayed and M. A. El-Sayed, *Laser. Med. Sci.*, 2008, **23**, 217–228.

15 D. Jaque, L. Martínez Maestro, B. del Rosal, P. Haro-Gonzalez, A. Benayas, J. L. Plaza, E. Martín Rodríguez and J. García Solé, *Nanoscale*, 2014, **6**, 9494.

16 J. A. Webb and R. Bardhan, *Nanoscale*, 2014, **6**, 2502.

17 L. Chomicz, J. Leszczynski and J. Rak, *J. Phys. Chem. B*, 2013, **117**, 8681–8688.

18 M. Wieczór, P. Wityk, J. Czub, L. Chomicz and J. Rak, *Chem. Phys. Lett.*, 2014, **595–596**, 133–137.

19 Y. Park, K. Polska, J. Rak, J. R. Wagner and L. Sanche, *J. Phys. Chem. B*, 2012, **116**, 9676–9682.

20 J. Rackwitz, J. Kopyra, I. Dąbkowska, K. Ebel, M. L. Ranković, A. R. Milosavljević and I. Bald, *Angew. Chem., Int. Ed.*, 2016, **55**, 10248–10252.

21 I. Bald, J. Langer, P. Tegeder and O. Ingólfsson, *Int. J. Mass Spectrom.*, 2008, **277**, 4–25.

22 B. Boudaïffa, *Science*, 2000, **287**, 1658–1660.

23 H. Abdoul-Carime, M. A. Huels, F. Brüning, E. Illenberger and L. Sanche, *J. Chem. Phys.*, 2000, **113**, 2517.

24 R. Schürmann and I. Bald, *J. Phys. Chem. C*, 2016, **120**, 3001–3009.

25 S. Cecchini, S. Girouard, M. A. Huels, L. Sanche and D. J. Hunting, *Radiat. Res.*, 2004, **162**, 604–615.

26 A. Keller, J. Rackwitz, E. Cauët, J. Liévin, T. Körzdörfer, A. Rotaru, K. V. Gothelf, F. Besenbacher and I. Bald, *Sci. Rep.*, 2014, **4**, 7391.

27 K. Watanabe, D. Menzel, N. Nilius and H.-J. Freund, *Chem. Rev.*, 2006, **106**, 4301–4320.

28 C. Boerigter, U. Aslam and S. Linic, *ACS Nano*, 2016, **10**, 6108–6115.

29 M. Pagliai, S. Caporali, M. Muniz-Miranda, G. Pratesi and V. Schettino, *J. Phys. Chem. Lett.*, 2012, **3**, 242–245.

30 R. Kopelman, *Science*, 1988, **241**, 1620–1626.

31 T. L. Thompson and J. T. Yates, *J. Phys. Chem. B*, 2006, **110**, 7431–7435.

32 T. Kim, C.-H. Lee, S.-W. Joo and K. Lee, *J. Colloid Interface Sci.*, 2008, **318**, 238–243.

33 D. A. Weitz and M. Oliveria, *Phys. Rev. Lett.*, 1984, **52**, 1433–1436.

34 Private communication with Dr Iwona Dąbkowska.

35 P. C. do Couto, B. J. Costa Cabral and S. Canuto, *Chem. Phys. Lett.*, 2006, **429**, 129–135.

36 N. Camillone, K. A. Khan, P. J. Lasky, L. Wu, J. E. Moryl and R. M. Osgood, *J. Chem. Phys.*, 1998, **109**, 8045.

37 E. P. Marsh, T. L. Gilton, W. Meier, M. R. Schneider and J. P. Cowin, *Phys. Rev. Lett.*, 1988, **61**, 2725–2725.

38 Z. Zhang, T. Deckert-Gaudig, P. Singh and V. Deckert, *Chem. Commun.*, 2015, **51**, 3069–3072.

39 P. C. Lee and D. Meisel, *J. Phys. Chem.*, 1982, **86**, 3391–3395.